Fig. 5.   Update weights versus time with the Q-modification controller.

excitation it can be shown that the update weights of the Q-modification controller converge to the ideal weights [20].

IV. CONCLUSION

In this brief, we presented a new and novel neuroadaptive controller architecture for nonlinear discrete-time uncertain systems based on the approach introduced in [20]. As in the continuous-time case, this controller architecture provided fast adaptation to effectively suppress system uncertainty while avoiding large parameter (high gain) stabilization which can excite unmodeled system dynamics. Extensions of the present approach to nonlinear in the parameters neural networks as well as output feedback control follow as in [20].

REFERENCES

[1] F. C. Chen and H. K. Khalil, "Adaptive control of nonlinear systems using neural networks," *Int. J. Contr.*, vol. 55, no. 6, pp. 1299–1317, 1992.

[2] F. C. Chen and H. K. Khalil, "Adaptive control of a class of nonlinear discrete-time systems using neural networks," *IEEE Trans. Autom. Contr.*, vol. 40, no. 5, pp. 791–807, May 1995.

[3] H. Deng, H.-X. Lin, and Y.-H. Wu, "Feedback-linearization-based neural adaptive control for unknown nonaffine nonlinear discrete-time systems," *IEEE Trans. Neural Netw.*, vol. 19, no. 9, pp. 1615–1625, Sep. 2008.

[4] S. S. Ge, T. H. Lee, G. Y. Li, and J. Zhang, "Adaptive NN control for a class of discrete-time non-linear systems," *Int. J. Contr.*, vol. 76, no. 4, pp. 334–354, 2003.

[5] W. M. Haddad and V. Chellaboina, *Nonlinear Dynamical Systems and Control: A Lyapunov-Based Approach*. Princeton, NJ: Princeton Univ. Press, 2008.

[6] K. J. Hunt, D. Sbarbaro, R. Zbikowski, and P. J. Gawthrop, "Neural networks for control: A survey," *Automatica*, vol. 28, pp. 1083–1112, Nov. 1992.

[7] C.-L. Hwang and C.-H. Lin, "A discrete-time multivariable neuroadaptive control for nonlinear unknown dynamic systems," *IEEE Trans. Syst. Man Cybern.*, vol. 30, no. 6, pp. 865–877, Dec. 2000.

[8] S. Jagannathan and F. L. Lewis, "Multilayer discrete-time neural net controller with guaranteed performance," *IEEE Trans. Neural Netw.*, vol. 7, no. 1, pp. 107–130, Jan. 1996.

[9] S. Jagannathan, "Control of a class of nonlinear discrete-time systems using multilayer neural networks," *IEEE Trans. Neural Netw.*, vol. 12, no. 5, pp. 1113–1120, Sep. 2001.

[10] S. Jagannathan, *Neural Network Control of Nonlinear Discrete-Time Systems*. Boca Raton, FL: CRC, 2006.

[11] A. U. Levin and K. S. Narendra, "Control of nonlinear dynamical systems using neural networks: Controllability and stabilization," *IEEE Trans. Neural Netw.*, vol. 4, no. 2, pp. 192–206, Mar. 1993.

[12] F. L. Lewis, S. Jagannathan, and A. Yesildirak, *Neural Network Control of Robot Manipulators and Nonlinear Systems*. London, U.K.: Taylor and Francis, 1999.

[13] L. Lin, P. N. Nikiforuk, and M. M. Gupta, "Fast neural learning and control of discrete-time nonlinear systems," *IEEE Trans. Syst. Man Cybern.*, vol. 25, no. 3, pp. 478–488, Mar. 1995.

[14] K. S. Narendra and K. Parthasarathy, "Identification and control of dynamical systems using neural networks," *IEEE Trans. Neural Netw.*, vol. 1, no. 1, pp. 4–27, Mar. 1990.

[15] J. Park and I. Sandberg, "Universal approximation using radial basis function networks," *Neural Comput.*, vol. 3, no. 2, pp. 246–257, 1991.

[16] M. Polycarpou, "Stable adaptive neural control scheme for nonlinear systems," *IEEE Trans. Autom. Contr.*, vol. 41, no. 3, pp. 447–451, Mar. 1996.

[17] R. Sanner and J. Slotine, "Gaussian networks for direct adaptive control," *IEEE Trans. Neural Netw.*, vol. 3, no. 6, pp. 837–864, Nov. 1992.

[18] J. Spooner, M. Maggiore, R. Ordonez, and K. Passino, *Stable Adaptive Control and Estimation for Nonlinear Systems: Neural and Fuzzy Approximator Techniques*. New York: Wiley, 2002.

[19] K. Volyanskyy, W. M. Haddad, and A. J. Calise, "A new neuroadaptive control architecture for nonlinear uncertain dynamical systems: Beyond σ and e-modifications," in *Proc. IEEE Conf. Dec. Contr.*, Cancun, Mexico, Dec. 2008, pp. 80–85.

[20] K. Y. Volyanskyy, W. M. Haddad, and A. J. Calise, "A new neuroadaptive control architecture for nonlinear uncertain dynamical systems: Beyond σ and e-modifications," *IEEE Trans. Neural Netw.*, vol. 20, no. 11, pp. 1707–1723, Nov. 2009.

Real-Time Simulation of Biologically Realistic Stochastic Neurons in VLSI

Hsin Chen, *Member, IEEE,* Sylvain Saïghi, *Member, IEEE,* Laure Buhry, and Sylvie Renaud, *Member, IEEE*

Abstract—Neuronal variability has been thought to play an important role in the brain. As the variability mainly comes from the uncertainty in biophysical mechanisms, stochastic neuron models have been proposed for studying how neurons compute with noise. However, most papers are limited to simulating stochastic neurons in a digital computer. The speed and the efficiency are thus limited especially when a large neuronal network is of concern. This brief explores the feasibility of simulating the stochastic behavior of biological neurons in a very large scale integrated (VLSI) system, which implements a programmable and configurable Hodgkin-Huxley model. By simply injecting noise to the VLSI neuron, various stochastic behaviors observed in biological neurons are reproduced realistically in VLSI. The noise-induced variability is further shown to enhance the signal modulation of a neuron. These results point toward the development of analog VLSI systems for exploring the stochastic behaviors of biological neuronal networks in large scale.

Index Terms—Analog VLSI, Hodgkin-Huxley formalism, neuromorphic VLSI, noise, stochastic behavior, stochastic neurons.

I. INTRODUCTION

Biological neurons have been found noisy both in the generation of spikes and in the transmission of synaptic signals. The noise comes from the random openings of ion channels, the quantal releases of neural transmitters, the coupling of background neural activity, etc. [19], [25]. As the noise affects neural computation directly, it has been of great interest to study how neurons compute with noise reliably [24]. Interestingly, many studies have indicated that noise plays a beneficial role at least by:

1) inducing neuronal variability [7];
2) enhancing the sensitivity of neurons to environmental stimuli [26];
3) inducing synchronization between neurons [1];
4) facilitating probabilistic inference according to the Bayes' rule in the brain [16].

The effect on synchrony could further relate to neural disorders such as Parkinson's disease [11] and hearing loss [4]. Understanding the effect of noise is thus crucial both for computational neuroscience and for improving the treatments to these neural diseases.

One major approach of theoretical studies is adding white noise to the biologically plausible, deterministic Hodgkin-Huxley (HH) model [12], either to the dynamics of gating variables of different ion channels, or to the dynamics of the membrane potential [9], [20]. As a result, the neuronal dynamics are modeled by stochastic differential equations (SDEs). This leads to at least two challenges for computer-based studies. First, the maximum number of neurons or SDEs a computer simulation can consider is limited. Many simplified models have thus been proposed [10], [13], However, the parameters of these models no longer relate to real biophysical properties directly, making it more difficult to extract parameter values, or to understand how different parameters affect neuronal behaviors. The second challenge is that the suggestions drawn from theoretical studies are not easy to verify with biological neurons, owing to the difficulty in manipulating a specific property of biological neurons independently.

Contrary to computer simulation, analog circuits are inherently suitable for simulating differential equations in real-time and in parallel [3]. By the merit of the natural, differential current–voltage relationship of a capacitor, noise-induced stochastic dynamics can be simulated by simply applying a noise current to the capacitor and measuring its corresponding voltage dynamics. The hardware simulation further facilitates the building of a hybrid network incorporating both very large scale integrated (VLSI) and biological neurons, allowing the network behavior to be studied efficiently by tuning the properties of VLSI neurons [15]. Therefore, this brief explores the feasibility of simulating different types of stochastic neurons in an analog VLSI system called the *Pamina*, which realizes the conductance-based HH model and runs in biologically realistic time [21].

II. HODGKIN-HUXLEY MODEL IN VLSI

Fig. 1(a) shows the *Pamina* chip [21] containing two HH-type neurons. Let C_M represent the membrane capacitance, and V_M the membrane voltage. Each neuron implements the formalism $C_M(dV_M/dt) = -\sum_i I_{ion,i} + \sum_j I_{syn,j} + I_{stim}$, where $I_{ion,i}$ represents an ionic current, $I_{syn,j}$ a synaptic current, and I_{stim} the stimulating input. The general form of $I_{ion,i}$ is given as

$$I_{ion,i} = g_i \cdot x^p \cdot y^q \cdot (V_M - E_i) \qquad (1)$$

where g_i and E_i are the maximum conductance and the reversal potential of the ionic current, respectively. x is the gating variable modeling the fraction of ion channels that are activated, while y the gating variable modeling the fraction of ion channels that are inactivated. Let λ represent either x or y. The dynamics of λ are guided by

$$\tau_\lambda \cdot \frac{d\lambda}{dt} = \lambda_\infty(V_M) - \lambda \qquad (2)$$

$$\lambda_\infty(V_M) = \frac{1}{1 + \exp(-(V_M - V_{off,\lambda})/V_{slope,\lambda})}. \qquad (3)$$

The minus sign in front of $(V_M - V_{off,\lambda})$ is omitted for the inactivation variable y. τ_λ is the time constant for approaching $\lambda_\infty(V_M)$. Although τ_λ is a function of V_M in the original HH model, it is a constant value in the *Pamina* chip to simplify circuit design. $V_{off,\lambda}$ and $V_{slope,\lambda}$ control the offset and the slope of the sigmoid function, respectively.

As shown in Fig. 1(b), each *Pamina* neuron contains five ionic currents, eight synaptic inputs, and one stimulating input. The five ionic conductances include the sodium current (I_{Na}), the potassium current (I_K), the leakage current (I_{leak}), the calcium current (I_{Ca}), and the calcium-dependent potassium current ($I_{K(Ca)}$). (p, q) for I_{Ca} allows users to select between (2, 1) and (1, 0), and the function $m(V_M, [Ca^{2+}])$ is realized in accordance with [14]. For the synaptic current, the dynamics of $r(V_{pre,j})$ also obey (2) and (3) with V_M replaced by the presynaptic potential $V_{pre,j}$ [6]. As $I_{syn,j}$ and I_{stim} have the same form as $I_{ion,i}$, all the conductances are implemented with a library of the analog operators detailed in [21]. Finally, V_{stim} and $V_{pre,j}$ are externally applied voltage.

The parameters of all the conductances are stored in the analog *parameter memory* [Fig. 1(a)], and the types of conductances or synapses connected to each neuron are controlled by the digital data stored in the *topology memory*. By integrating the *Pamina* chip with a field-programmable-gate-array and data converters on a customized peripheral-component-interconnect (PCI) card, the neurons can be configured and recorded easily through C programming in a computer. Compared to other conductance-based neurons in VLSI [8], [22], the *Pamina* chip has the advantages that all neuronal parameters are dynamically tunable over a wide range, together with a flexible topology. These features make the chip particular suitable for exploring the stochastic behaviors observed in different biological neurons.
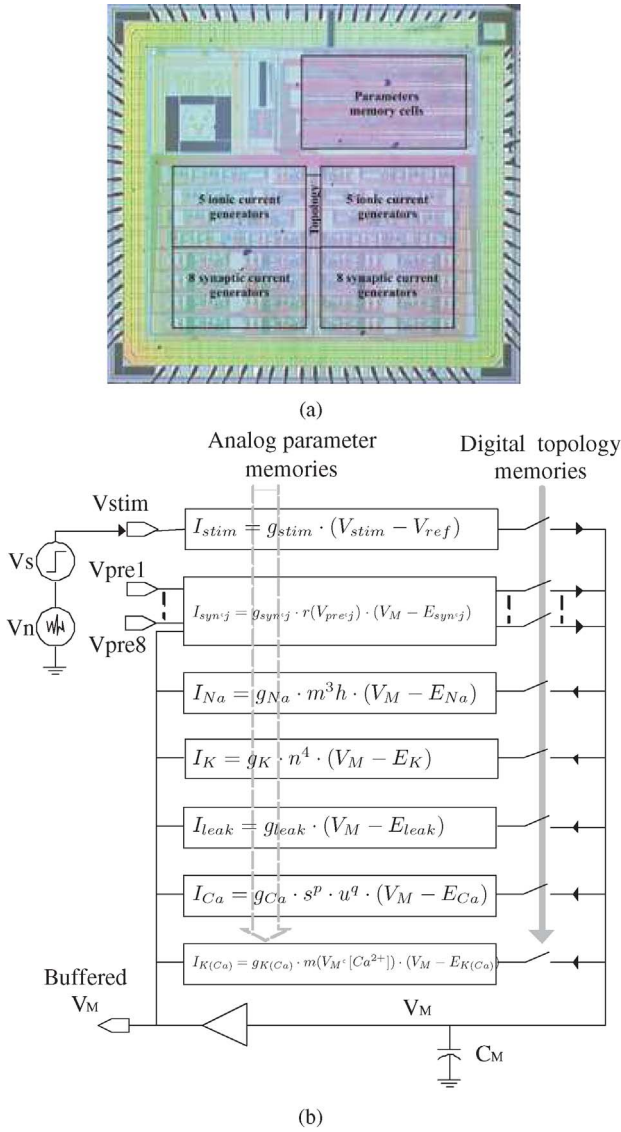
(a)

(b)

Fig. 1. (a) Microphotograph of the *Pamina* chip fabricated with the 0.35 μm BiCMOS technology by the Austriamicrosystems. The chip area is 4170 × 3480 μm^2. (b) Block diagram of a neuron.

III. MAPPING BIOLOGICAL MODELS INTO VLSI

A. Parameter Extraction

The minimal HH model proposed in [18] is of our particular interests, as different classes of cortical and thalamic neurons have been modeled satisfactorily with a minimal number of ionic conductances. In addition, the conductance models in [18] are similar to those implemented in the *Pamina* chip, allowing most parameters to be adopted directly for VLSI simulation according to the mappings described as follows.

All voltage levels in the VLSI neuron are designed to be five times greater than their corresponding values in biological neurons, i.e., $V_{\text{VLSI}} = 5 * V_{\text{BIO}}$, while the time scale is identical for both VLSI and biological neurons. Let C_{VLSI} and C_{BIO} represent the membrane capacitances of VLSI and biological neurons, respectively. The conductance mapping is proportional to the capacitance ratio as $g_{\text{VLSI}}/g_{\text{BIO}} = C_{\text{VLSI}}/C_{\text{BIO}}$. The current mapping then equals the product of the voltage

TABLE I
PARAMETERS OF DIFFERENT NEURONS SIMULATED IN VLSI

	FS neuron	RS neuron	LTS neuron
C_M ($\mu F/cm^2$)	1	1	1
Area (cm^2)	14×10^{-5}	29×10^{-5}	29×10^{-5}
g_{stim} (mS/cm^2)	1.08	1.08	1.08
g_{Na} (mS/cm^2)	44	44	44
E_{Na} (mV)	50	50	50
τ_m (ms)	0.07	0.07	0.07
$V_{\text{off},m}$ (mV)	−34.42	−34.42	−34.42
$V_{\text{slope},m}$ (mV)	6.47	6.47	6.47
τ_h (ms)	0.36	0.36	0.36
$V_{\text{off},h}$ (mV)	−39.07	−39.07	−39.07
$V_{\text{slope},h}$ (mV)	3.932	3.932	3.932
g_K (mS/cm^2)	10	10	5–10
E_K (mV)	−90	−90	−90
τ_n (ms)	1	1	1
$V_{\text{off},n}$ (mV)	−29.08	−29.08	−29.08
$V_{\text{slope},n}$ (mV)	7.854	7.854	7.854
g_{leak} (mS/cm^2)	0.1	0.1	0.1
E_{leak} (mV)	−70	−70	−70
g_{Ca} (mS/cm^2)	–	0.35	2
E_{Ca} (mV)	–	−90	120
τ_s (ms)	–	200	0.65
$V_{\text{off},s}$ (mV)	–	−35	−115
$V_{\text{slope},s}$ (mV)	–	10	6.2
τ_u (ms)	–	–	100
$V_{\text{off},u}$ (mV)	–	–	−120
$V_{\text{slope},u}$ (mV)	–	–	16

and conductance mappings, i.e., $I_{\text{VLSI}}/I_{\text{BIO}} = 5 * C_{\text{VLSI}}/C_{\text{BIO}}$. In the *Pamina* chip, $C_{\text{VLSI}} = 5$nF and the biological neurons have $C_{\text{BIO}} = C_M \cdot$ Area with C_M and Area given in Table. I.

The only difference between the VLSI and biological neurons is that the dynamics of gating variables in [18] are modeled as $d\lambda/dt = \alpha_\lambda(V_M) \cdot (1 - \lambda) - \beta_\lambda(V_M) \cdot \lambda$ instead of (2). The parameters τ_λ, $V_{\text{off},\lambda}$, and $V_{\text{slope},\lambda}$ are thus extracted by:

1) calculating $\alpha_\lambda(V_M)$ and $\beta_\lambda(V_M)$ over the range $V_M = [-100, 100]$ mV;
2) deriving $\lambda_\infty(V_M)$ according to $\lambda_\infty = \alpha_\lambda/(\alpha_\lambda + \beta_\lambda)$;
3) setting the V_M corresponding to $\lambda_\infty = 0.5$ as $V_{\text{off},\lambda}$;
4) and then extracting $V_{\text{slope},\lambda}$ at a specific λ_∞.

In addition, τ_λ is simply calculated from $\tau_\lambda(V_M) = [\alpha_\lambda(V_M) + \beta_\lambda(V_M)]^{-1}$ at $V_M = -70$ mV.

Three types of neurons, the *fast-spiking* (FS) neurons, the *Regular-Spiking* (RS) neurons, and the *low-threshold-spiking* (LTS) neurons were simulated in our experiments. Table I summarized the parameter values extracted from [18]. For the RS neuron, the calcium conductance (I_{Ca}) was programmed to realize the slow potassium current (I_M) with $(p, q) = (1, 0)$. For the LTS neuron, $(p, q) = (2, 1)$ and $\tau_s = 0.65$ ms were set to realize the low-threshold calcium current (I_T) in [18].

B. Noise Injection

While the stochastic behaviors of biological neurons were reproduced with remarkable precision in [20] by adding white noise ($\sigma \cdot W(t)$) to the kinetics of gating variables, the Pamina chip originally designed for simulating deterministic HH models only allowed the noise to be added to the kinetics of
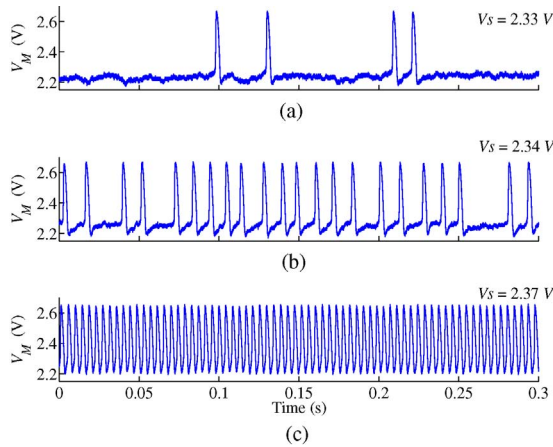
Fig. 2. Responses of a stochastic FS neuron in VLSI with $V_n = 800\,\text{mV}_\text{pp}$ and (a) $V_S = 2.33$-V, (b) $V_S = 2.34$-V, (c) $V_S = 2.37$-V.

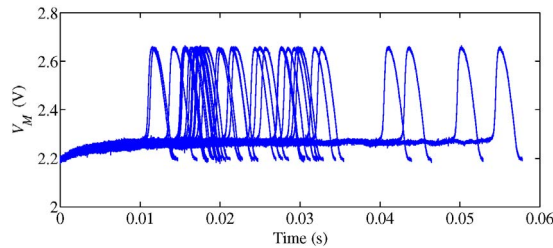
Fig. 3. Superimpose of 37 spikes generated by a stochastic FS neuron in VLSI with $V_S = 2.34$--V and $V_n = 800\,\text{mV}_\text{pp}$.

the membrane voltage as (4)

$$C_M \frac{dV_M}{dt} = -\sum_i I_{\text{ion},i} + \sum_j I_{\text{syn},j} + I_{\text{stim}} + \sigma \cdot W(t). \quad (4)$$

Let $V_M = V_{Md} + V_{Ms}$, with V_{Md} and V_{Ms} representing the deterministic and the stochastic components, respectively. By Taylor expansion, $\lambda_\infty(V_{Md} + V_{Ms})$ can be expressed as

$$\lambda_\infty(V_{Md} + V_{Ms}) = \lambda_\infty(V_{Md}) + \lambda'_\infty(V_{Md}) \cdot V_{Ms} + o(V_{Ms}) \quad (5)$$

where $o(V_{Ms})$ represents high-order terms of V_{Ms}. Equation (5) indicates that although the white noise in (4) can be transferred to the dynamics of λ in (2) via V_M, the transferred noise, $\lambda'_\infty(V_{Md}) \cdot V_{Ms} + o(V_{Ms})$, is no longer white due to the filtering effect by (4). Furthermore, V_{Ms} is nonlinearly transformed by the sigmoid function. Adding white noise to the kinetics of V_M could thus result in different responses from adding white noise to the kinetics of λ.

With this note in mind, we superimposed the noise signal V_n on the stimulating signal V_S in the *Pamina* chip to obtain $V_{\text{stim}} = V_S + V_n$ [Fig. 1(b)]. V_{stim} was then converted into the current $I_{\text{stim}} = g_{\text{stim}}(V_{\text{stim}} - V_{\text{ref}})$, wherein the stochastic component of I_{stim} corresponded to $\sigma \cdot W(t)$ in (4). The effect of the noise on different types of neurons was then explored and discussed as follows.
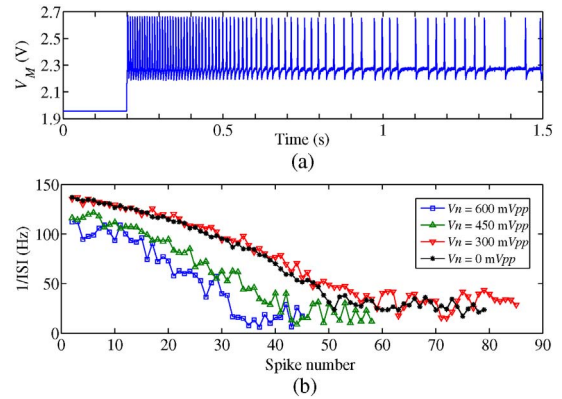

Fig. 4. (a) Response of a stochastic RS neuron in VLSI to a step-input stimulation rising from $V_S = 1.3$-V to $V_S = 2.4$-V at $t = 0.2$ s. (b) Inverse of inter-spike-interval of a stochastic RS neuron in VLSI in response to the same depolarizing stimulation lasting for 1600 ms with various levels of noise.

IV. SIMULATING STOCHASTIC NEURONS IN VLSI

A. Fast-Spiking Neurons

The FS neuron is a major class of neurons in the cerebral cortex, involving only I_{Na}, I_K, and I_{leak}. In the absence of noise injection, the FS neuron simulated in the *Pamina* chip generates spikes only when $V_S \geq 2.34$-V. With $V_n = 800\,\text{mV}_\text{pp}$ superimposed on V_S, the measured responses of the FS neuron to:

1) subthreshold ($V_S = 2.33$-V);
2) suprathreshold[1] ($V_S = 2.34$-V);
3) above-threshold ($V_S = 2.37$-V) stimulation are shown in Fig. 2.

Under subthreshold stimulation, the noise induced spontaneous firings. Suprathreshold stimulation then leads to increased spiking frequency and reduced frequency variation. As V_S is well above the threshold, the spiking frequency approaches constant while the spiking amplitude remains slightly variable due to the presence of noise. These phenomena have been reported in biological experiments both *in vivo* and *in vitro* [2], [5].

As V_M is polarized to around the same minimum voltage after each spike generation, the minimum voltage can be thought of as the initial state from which the neuron is discharged by V_S of generate the next spike. Fig. 3 superimposes 37 spikes generated under the suprathreshold stimulation, aligning their initial states with $t = 0$. With a constant V_S, the time required for discharging the membrane over the spiking threshold varies from one spike to another. Such noise-induced variability has been widely observed in biological neurons [17]. Although the variability could impede neurons from coding information as spike timing precisely, it has been found useful for auditory neurons, for example, to encode distinct features efficiently [4]. Therefore, the results here demonstrate the feasibility of reproducing the stochastic behaviors of biologically realistic neurons in VLSI by simply adding noise to the neuronal membrane.

---

[1]The quantitative definition for suprathreshold stimulation is that the probability of generating spikes under suprathreshold stimulation is 0.5 [25].
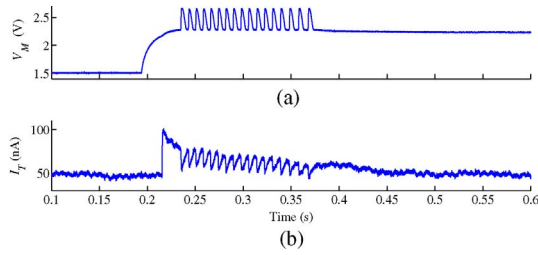
Fig. 5. (a) V_M and (b) I_T of a LTS neuron in VLSI in response to a hyperpolarizing stimulation which was dismissed by changing $V_S = 2.22$-V to $V_S = 2.3$-V at $t = 0.2$ s.
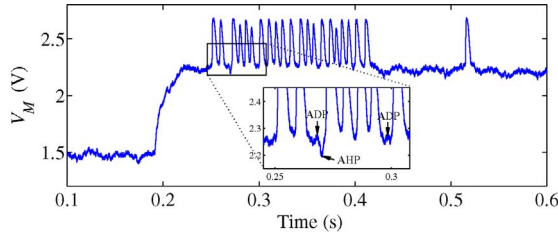

Fig. 6. Responses of a LTS neuron in VLSI to $V_n = 1.8$ V_{pp} superimposed on a hyperpolarizing stimulation which was dismissed abruptly by changing $V_S = 2.22$-V to $V_S = 2.3$-V at $t = 0.2$ s.

Fig. 7. Responses of a FS neuron to (a) sinusoidal and (b) square inputs with an offset of 2.34-V and an amplitude of 30 mV. The V_{stim} has been shifted by -0.7-V.

Fig. 8. Statistical firing probability of a deterministic FS neuron in response to (a) sinusoidal and (b) square waves.

B. Regular-Spiking Neurons

The RS neuron has been the largest class of neurons in the neocortex. The slow potassium current (I_M) is activated by the depolarization of neuronal membranes. Once activated, I_M functions as an extra polarizing current, causing the spiking frequency to adapt toward a minimum.

With V_S stepping from 1.3-V (inhibition) to 2.4-V (above threshold) at $t = 0.2$ s and $V_n = 300$ mV_{pp}, the measured responses of the stochastic RS neuron in the *Pamina* chip are shown in Fig. 4(a). The frequency adaptation is clearly shown, and the noise distorts the spiking frequency during adaptation. Let the inverse of the inter-spike-interval (ISI) between consecutive spikes approximate the instantaneous spiking frequency. Fig. 4(b) plots the spiking frequency of the RS neuron during 1600 ms of the above-threshold stimulation ($V_S = 2.4$-V). Without noise, the spiking frequency adapts from 137 Hz to 25 Hz gradually. The variability around 25 Hz is attributed to the clockfeedthroughs in the PCI system. As the noise is increased, the adaptation process becomes distorted. The initial firing frequency further reduces when V_n is greater than 300 mV_{pp}, owing to the serious threshold variations induced by the noise. On the contrary, the adaptation rate is nearly constant for different V_n. This is because I_M with a large τ_s (200 ms) is less affected by noise.

This experiment demonstrates that the effect of noise can be studied efficiently by VLSI simulation in real-time, and the same should hold as a large network of neurons is of concern. Although software tools such as NEURON can also complete the simulation in Fig. 4(a) within negligible time, the time required would increase dramatically as the number of neurons grows.
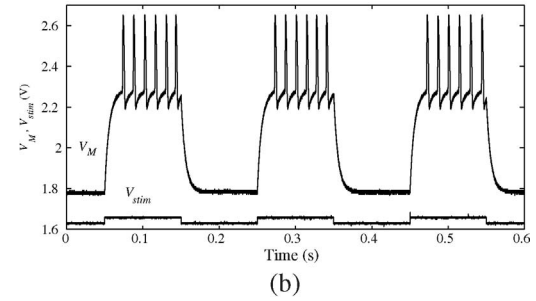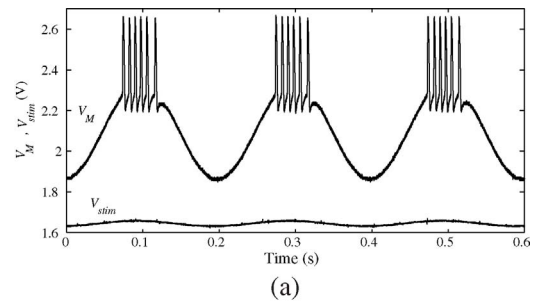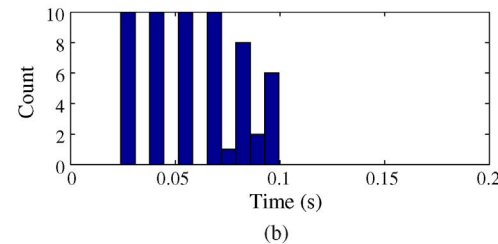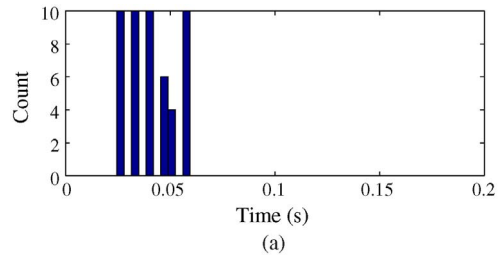
C. Low-Threshold-Spiking Neurons

The major distinctive behavior of the LTS neuron is the generation of a burst of spikes at the "off-set" of a hyperpolarizing current stimulus. This property has been shown related to the low-threshold calcium current (I_T). With the *Pamina* chip programmed to simulate the LTS neuron, the neuron generates post-inhibitory rebounds after the release of a hyperpolarizing stimulation (at $t = 0.2$ s), as shown in Fig. 5. The corresponding I_T is shown to function as a depolarizing current, inducing the spikes during its slow inactivation.

As $V_n = 1.8 V_{pp}$ is superimposed on the same hyperpolarizing stimulation, the LTS neuron responds as shown in Fig. 6. Before the hyperpolarization ended ($t < 0.2$ s), the neuron generates no spikes even if the noise amplitude plus the hy-
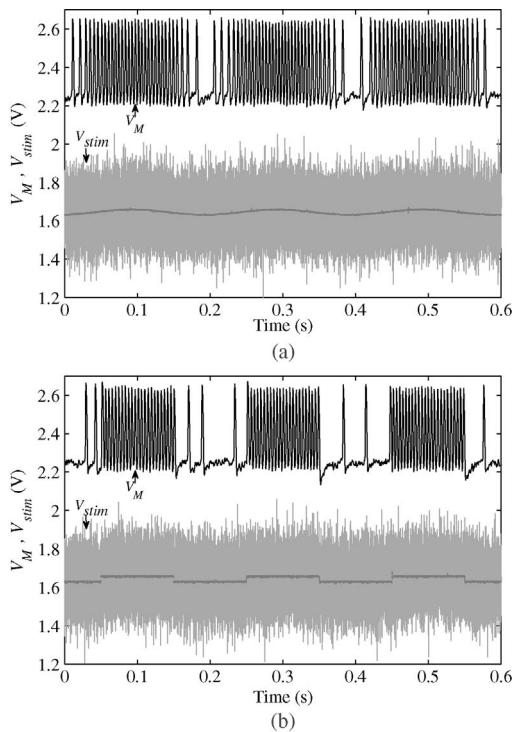
Fig. 9. Responses (V_M) of a stochastic FS neuron with $V_n = 800\,\text{mV}_{\text{pp}}$ superimposed on (a) sinusoidal and (b) square stimuli, V_S. The total input $V_{\text{stim}} = V_S + V_n$ has been shifted by -0.7-V in the plots.

perpolarizing stimulation already exceeds the firing threshold (2.34-V). This is because the noise has a maximum amplitude with a very low likelihood and in a short period of time. After $t > 0.2s$, the post-inhibitory rebounds are evoked by the stimulation off-set, but the spiking frequency is distorted. The magnified window further reveals dynamics analogous to the afterdepolarization (ADP) and afterhyperpolarization (AHP) observed in biological neurons. The ADP and AHP could play an important role in affecting the synaptic plasticity in the hippocampus [23] and has been simulated with a more complex HH model with noise added to gating variables in [20]. The feasibility of simulating sophisticated stochastic behaviors such as ADP and AHP in real-time in VLSI is thus demonstrated. Nevertheless, adding noise to the gating variables would be much more effective, as discussed in Section III-B.

D. Noise-Enhanced Signal Modulation

Except for the rich stochastic behaviors explored above, noise has been shown useful for enhancing neurons' sensitivity to weak signals by the mechanism called *stochastic resonance* [26]. We here demonstrate the noise-enhanced sensitivity as the responses of a stochastic FS neuron to two weak stimuli, one with a sinusoidal waveform and the other with a square waveform. Both stimuli have an amplitude of 30 mV, an offset of 2.34-V, and a frequency of 5 Hz. The offset level introduces suprathreshold stimulation to the neuron. Without noise, the neuron only fires when the stimulating waveform exceeds its firing threshold, as shown in Fig. 7. The firing frequency and the separation between consecutive groups of spikes are
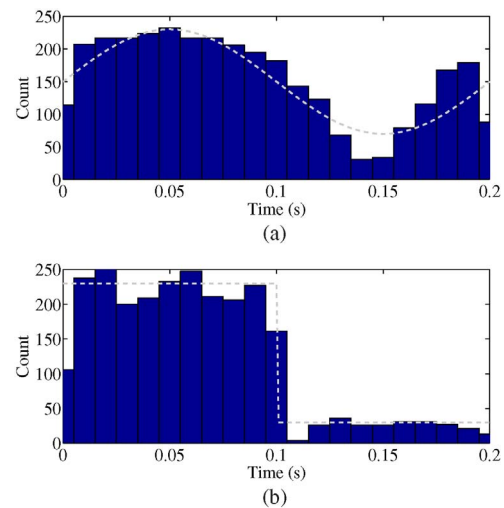

Fig. 10. Statistical firing probability of a stochastic FS neuron in response to (a) sinusoidal and (b) square waves.

very similar for both stimuli. Let the timing of each spike be calculated as its phase with respect to the stimulating waveforms. By recording the response to each stimulus for 2 s, the statistical distributions of the spike timing for both stimuli are obtained and shown in Fig. 8. The square waveform simply results in a wider distribution than the sinusoidal wave. Given the two spike trains are received by a post-synaptic neuron, the post-synaptic neuron could only detect the frequency but not the waveform of the stimuli.

By contrast, with $V_n = 800\,\text{mV}_{\text{pp}}$ added to the input, the FS neuron exhibits dramatically different responses, as shown in Fig. 9. Although the sinusoidal or square waveform is masked off by the large noise, the ISIs are modulated in accordance with the waveforms. From a prolonged recording of 20 s for each stimulus, Fig. 10 plots the statistical distributions of the spike timing for the two stimulating waveforms. The histograms reconstruct the waveforms of the input stimuli, indicating that the modulated ISIs allow post-synaptic neurons to perceive the waveforms from spike timing. The advantage and the utility of noise-induced stochastic behavior in neurons is first demonstrated in VLSI. Certainly, an optimum level of noise exists for maximizing the sensitivity, and the optimum level is different from one case to another.

V. CONCLUSION

This brief demonstrated the feasibility of simulating various stochastic neurons in VLSI by simply injecting noise into the membrane capacitor of a HH model in VLSI. Various stochastic behaviors observed in biological neurons have been reproduced in VLSI realistically. The effect of noise on different neurons has thus been studied efficiently. These promising results point toward the development of analog VLSI systems able to simulate stochastic neuronal networks in real or accelerated time. The influence of noise on synaptic connections and network behaviors will then be explored. In addition, hybrid silicon-neuron networks could be built to ease the investigation on how individual parameters affect stochastic neural computation, as well as to verify the suggestions

drawn from computer-based simulations. The understanding on how neurons compute with noise reliably would further inspire novel neuromorphic computation. For example, as the intrinsic noise of transistors will become nonnegligible in the deep-submicrometer era, it will be interesting to explore the possibility of using the intrinsic VLSI noise for computation like biological neurons do.

REFERENCES

[1] J. M. Casado, "Synchronization of two Hodgkin–Huxley neurons due to internal noise," *Phys. Lett. A*, vol. 310, nos. 5–6, pp. 400–406, 2003.
[2] P. Chadderton, T. W. Margrie, and M. Hausser, "Intergration of quanta in cerebellar granule cell during sensory processing," *Nature*, vol. 428, no. 6985, pp. 856–860, 2004.
[3] L. O. Chua, T. Roska, T. Kozek, and A. Zarandy, "CNN universal chips crank up the computing power," *IEEE Circuits Devices Mag.*, vol. 12, no. 4, pp. 18–28, Jul. 1996.
[4] J. J. Collins, C. C. Chow, and T. T. Imhoff, "Stochastic resonance without tuning," *Nature*, vol. 376, no. 6537, pp. 236–238, 1995.
[5] E. D'Angelo, G. De Filippi, P. Rossi, and V. Taglietti, "Ionic mechanism of electroresponsiveness in cerebellar granule cells implicates the action of a persistent sodium current," *J. Neurophysiol.*, vol. 80, no. 2, pp. 493–503, 1998.
[6] A. Destexhe, Z. F. Mainen, and T. J. Sejnowski, "Kinetic models of synaptic transmission," in *Methods in Neuronal Modeling*, C. Koch and I. Segev, Eds. Cambridge, MA: MIT Press, 1998.
[7] G. B. Ermentrout, R. F. Galán, and N. N. Urban, "Reliability, synchrony and noise," *Trends Neurosci.*, vol. 31, no. 8, pp. 428–434, 2008.
[8] E. Farquhar and P. Hasler, "A bio-physically inspired silicon neuron," *IEEE Trans. Circuits Syst. I, Reg. Papers*, vol. 52, no. 3, pp. 477–488, Mar. 2005.
[9] R. F. Fox, "Stochastic versions of the Hodgkin–Huxley equations," *Biophys. J.*, vol. 72, no. 5, pp. 2068–2074, 1997.
[10] W. Gerstner and W. M. Kistler, *Spiking Neuron Models*. Cambridge, U.K.: Cambridge University Press, 2002.
[11] C. Hammond, H. Bergman, P. Brown, "Pathological synchronization in Parkinson's Disease: Networks, models, and treatments," *Trends Neurosci.*, vol. 30, no. 7, pp. 357–364, Jul. 2007.
[12] A. L. Hodgkin and F. Huxley, "A quantitative description of membrane current and its application to conduction and excitation in nerve," *J. Physiol.*, vol. 117, no. 4, pp. 500–544, 1952.
[13] E. M. Izhikevich, "Which model to use for cortical spiking neurons?" *IEEE Trans. Neural Netw.*, vol. 15, no. 5, pp. 1063–1070, Feb. 2004.
[14] C. Koch, "Beyond Hodgkin and Huxley: Calcium and calcium-dependent potassium currents," in *Biophysics of Computation*, C. Koch, Ed. New York: Oxford University Press, 1999.
[15] G. Le Masson, S. Le Masson, D. Debay, and T. Bal, "Feedback inhibition controls spike transfer in hybrid thalamic circuits," *Nature*, vol. 417, no. 6891, pp. 854–858, 2002.
[16] W. J. Ma, J. M. Beck, P. E. Latham, and A. Pouget, "Bayesian inference with probabilistic population codes," *Nat. Neurosci.*, vol. 9, no. 11, pp. 1432–1438, 2006.
[17] C. Pecher, "La fluctuation d'excitabilité de la fibre nerveuse," *Arch. Int. Physiol. Biochem.*, vol. 49, pp. 129–152, 1939.
[18] M. Pospischil, M. Toledo-Rodriguez, C. Monier, Z. Piwkowska, T. Bal, Y. Fregnac, H. Markram, and A. Destexhe, "Minimal Hodgkin-Huxley type models for different classes of cortical and thalamic neurons," *Biol. Cybern.*, vol. 99, nos. 4–5, pp. 427–441, 2008.
[19] M. Rudolph and A. Destexhe, "An extended analytic expression for the membrane potential distribution of conductance-based synaptic noise," *Neural Comput.*, vol. 17, no. 11, pp. 2301–2315, 2005.
[20] A. Saarinen, M.-L. Linne, and O. Yli-Harja, "Modeling single neuron behavior using stochastic differential equations," *Neurocomputing*, vol. 69, nos. 10–12, pp. 1091–1096, 2006.
[21] S. Saïghi, J. Tomas, Y. Bornat, and S. Renaud, "A library of analog operators based on the Hodgkin-Huxley formalism for the design of tunable and real-time silicon neurons," *IEEE Trans. Biomed. Circuits Syst.*, 2010, submitted for published.
[22] M. F. Simoni, G. S. Cymbalyuk, M. E. Sorensen, R. L. Calabrese, and S. P. DeWeerth, "A multiconductance silicon neuron with biologically matched dynamics," *IEEE Trans. Biomed. Eng.*, vol. 51, no. 2, pp. 342–354, Feb. 2004.
[23] N. Spruston, "Pyramidal neurons: Dendritic structure and synaptic integration," *Nat. Rev. Neurosci.*, vol. 9, no. 3, pp. 206–221, 2008.
[24] R. B. Stein, E. R. Gossen, and K. E. Jones, "Neuronal variability: Noise or part of the signal?" *Nat. Rev. Neurosci.*, vol. 6, no. 5, pp. 389–397, 2005.
[25] J. A. White, J. T. Rubinstein, and A. R. Kay, "Channel noise in neurons," *Trends Neurosci.*, vol. 23, no. 3, pp. 131–137, 2000.
[26] K. Wiesenfeld and F. Moss, "Stochastic resonance and the benefits of noise: From ice ages to crayfish and squids," *Nature*, vol. 373, pp. 33–36, Jan. 1995.

Constructive Approximation to Multivariate Function by Decay RBF Neural Network

Muzhou Hou and Xuli Han

Abstract—It is well known that single hidden layer feedforward networks with radial basis function (RBF) kernels are universal approximators when all the parameters of the networks are obtained through all kinds of algorithms. However, as observed in most neural network implementations, tuning all the parameters of the network may cause learning complicated, poor generalization, overtraining and unstable. Unlike conventional neural network theories, this brief gives a constructive proof for the fact that a decay RBF neural network with $n+1$ hidden neurons can interpolate $n+1$ multivariate samples with zero error. Then we prove that the given decay RBFs can uniformly approximate any continuous multivariate functions with arbitrary precision without training. The faster convergence and better generalization performance than conventional RBF algorithm, BP algorithm, extreme learning machine and support vector machines are shown by means of two numerical experiments.

Index Terms—Constructive neural networks, decay radial basis function (RBF) neural networks, interpolation, uniformly approximation.

I. INTRODUCTION

THE WIDESPREAD popularity of neural networks in many fields is mainly due to their ability to approximate complex multivariate nonlinear functions directly from the input samples. Neural networks can provide models for a large class of natural and artificial phenomena that are difficult to handle using classical parametric techniques.

M. Hou is with the School of Mathematical Sciences and Computing Technology, Central South University, Changsha 410083, China, and also with the School of Information Science and Engineering, Central South University, Changsha 410083, China (e-mail: houmuzhou@sina.com).

X. Han is with the School of Mathematical Sciences and Computing Technology, Central South University, Changsha 410083, China (e-mail: xlhan@mail.csu.edu.cn).